

# Trajectory-based LQR Control of a Grid-connected Converter with an *LCL* Filter

Toit Mouton\* and Tobias Geyer\*\*

\* *Department of Electrical and Electronic Engineering, University of Stellenbosch, Private Bag X1, Matieland, 7602, South Africa (e-mail: dtmouton@sun.ac.za).*

\*\* *ABB Corporate Research, 5405 Baden-Dättwil, Switzerland (e-mail: t.geyer@ieee.org).*

---

**Abstract:** This paper proposes a trajectory-based controller for a pulse-width modulated high-power converter which connects to the power grid through an *LCL* filter. The controller is separated into a feed-forward controller, which takes the non-linear behaviour of the pulse-width modulator into account as well as a linear feedback controller. The linear feedback controller is a simple linear-quadratic regulator (LQR). One of the main advantages of this approach is the simplicity of the design of the LQR which only requires selecting the weights of the cost function. Simulation results show that the proposed approach exhibits excellent steady-state performance with fast response during transients.

*Keywords:* Control of switched systems, Grid-connected converters, Optimal control theory, Real-time control, Power electronics

---

## 1. INTRODUCTION

The use of *LCL* filters in grid-connected converters offers significantly higher attenuation of the switching harmonics than filters consisting of only series inductors. The main challenge when designing controllers for grid-connected converters with *LCL* filters is the fact that the *LCL* filter itself is a highly underdamped circuit. The issue of resonance damping has mainly been addressed through multi-loop control strategies (Dahono (2002), Loh and Holmes (2005), Parker et al. (2014)), the concept of virtual resistance (Dahono (2002), Dannehl et al. (2010)) and filter-based active damping strategies (Dannehl et al. (2010), Liserre et al. (2004)).

The concept of trajectory tracking is a well-known approach that provides accurate control of non-linear systems (Nieuwstadt and Murray (1997)). The underlying idea is to separate the controller into a non-linear feedforward compensator and a linear feedback compensator. The feedforward compensator takes the non-linear nature of the pulse-width modulator into consideration and synthesises a feasible state-space trajectory for the system given a desired reference signal as well as a set of nominal inputs that drive the system along this trajectory. The feedback compensator corrects for errors between the desired trajectory and the actual trajectory.

This paper proposes a trajectory-based control strategy for a pulse-width modulated grid-connected converter with an *LCL* filter. The feasible trajectory is calculated by taking the full non-linear behaviour of the pulse-width modulated loop into account. The feedback controller is a discrete-time linear-quadratic regulator (LQR) that acts as a small-signal controller to guide the system along

the reference trajectory. One of the main advantages of the proposed approach is the simplicity of the design of the LQR. It only requires the formulation of a suitable cost function and doesn't require any of the specialised approaches mentioned above.

Section 2.1 of this paper describes the system and derives the system of differential equations that describe the system. Section 2.2 summarizes the control problem, while section 2.3 describes the process of generating the feasible reference trajectories by taking the non-linear behaviour of the loop into account. A small-signal model of the pulse-width modulator is presented in section 2.4. This small-signal model gives rise to a linear discrete-time model of the small-signal control loop which is used to design the LQR in section 3.1. Section 3.2 contains a case study of a high-power grid-connected converter operating at a low switching frequency. Simulation results are presented to verify the operation of the proposed control strategy.

## 2. SYSTEM AND CONTROL PROBLEM

### 2.1 The system

Fig. 1 shows a three-phase two-level converter, which is connected to the power grid via an *LCL* filter. The dc-bus voltage  $V_d$  is assumed to be constant. The equivalent series resistances (ESR) of the filter inductor  $L$ , the filter capacitor  $C$  and the grid-side inductance  $L_g$  are denoted by  $R$ ,  $R_C$  and  $R_g$ , respectively. The three-phase converter output current, grid current, capacitor voltage, and grid voltage vectors are defined as:

$$\mathbf{i}_{abc} = \begin{bmatrix} i_a \\ i_b \\ i_c \end{bmatrix}, \mathbf{i}_{g,abc} = \begin{bmatrix} i_{ga} \\ i_{gb} \\ i_{gc} \end{bmatrix}, \mathbf{v}_{c,abc} = \begin{bmatrix} v_{ca} \\ v_{cb} \\ v_{cc} \end{bmatrix}, \mathbf{v}_{g,abc} = \begin{bmatrix} v_{ga} \\ v_{gb} \\ v_{gc} \end{bmatrix},$$

respectively.

Three-phase quantities  $\xi_{abc} = [\xi_a \ \xi_b \ \xi_c]^T$  in the  $abc$  reference frame are transformed to the  $\alpha\beta$  reference frame  $\xi = [\xi_\alpha \ \xi_\beta]^T$  by means of the transformation matrix

$$\xi = \frac{2}{3} \mathbf{P} \xi_{abc},$$

where

$$\mathbf{P} = \begin{bmatrix} 1 & -\frac{1}{2} & -\frac{1}{2} \\ 0 & \frac{\sqrt{3}}{2} & -\frac{\sqrt{3}}{2} \end{bmatrix}.$$

Conversely,  $\xi$  can be transformed from  $\alpha\beta$  to  $\xi_{abc}$  by means of

$$\xi_{abc} = \mathbf{P}^T \xi.$$

Note that, in order to simplify the notation, vectors without any subscripts represent variables in the  $\alpha\beta$  reference frame.

The converter switching state  $\mathbf{p}_{abc}$  is denoted by

$$\mathbf{p}_{abc} = [p_a \ p_b \ p_c]^T, \text{ where } p_a, p_b, p_c \in \{-1, 1\}.$$

The three converter output voltages are related to the switching state by

$$[v_{an} \ v_{bn} \ v_{cn}]^T = \frac{V_d}{2} [p_a \ p_b \ p_c]^T.$$

The continuous-time dynamics of the system are described by

$$\dot{\mathbf{x}} = \mathbf{F} \mathbf{x} + \mathbf{G} \mathbf{p} + \mathbf{H} \mathbf{v}_g, \quad (1)$$

where the state-vector is defined as  $\mathbf{x} = [i^T \ i_g^T \ v_c^T]^T$ . The expressions for  $\mathbf{F}$ ,  $\mathbf{G}$  and  $\mathbf{H}$  can be found in appendix A.

## 2.2 The control problem

The aim of the controller is to control the grid currents  $i_{ga}$ ,  $i_{gb}$  and  $i_{gc}$  in such a way that the desired real and reactive power is delivered to or drawn from the grid. Other consideration are the harmonic content of the grid current, the transient response of the controller and robustness to variations in system parameters.

Fig. 2 shows a block diagram of the proposed trajectory-based controller. The gating signals for the three-phase converter are generated by three asymmetrically-regularly-sampled (double-update) digital pulse-width modulators with a single triangular carrier (see Holmes and Lipo (2003)). Fig. 3 shows the PWM waveforms. The sampling instants of the digital control loop occur at the upper and lower peaks of the carrier. The sampling period  $T$  is thus

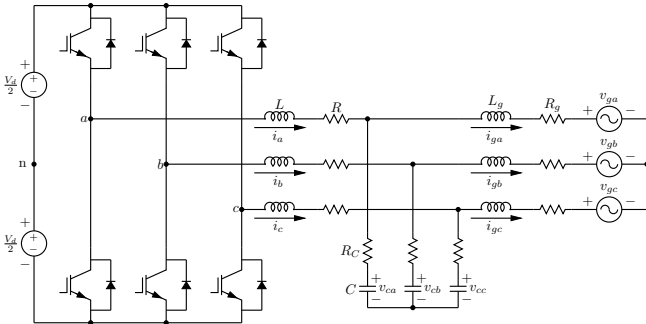


Fig. 1. Three-phase two-level DC-to-AC converter which is connected to the power grid by means of an  $LCL$  filter.

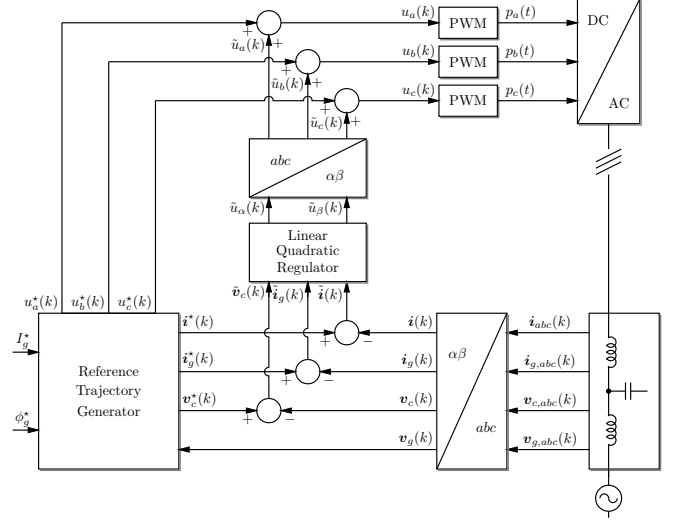


Fig. 2. Block diagram of the trajectory-based controller.

equal to half the switching period  $T_s$  of the converter. The switching frequency  $f_s$  of the converter is defined as  $f_s = \frac{1}{T_s}$ . It is assumed that the triangular carrier has an amplitude of 1.

The two reference signals  $I_g^*$  and  $\phi_g^*$  denote the amplitude and phase of the required sinusoidal grid currents. It is assumed that  $I_g^*$  and  $\phi_g^*$  are constant or change slowly relative to the grid frequency. In a practical system where  $V_d$  is not necessarily fixed, an outer loop controller, typically containing a proportional integral (PI) controller, can be used to generate these reference signals.

The block entitled “Reference Trajectory Generator” generates the steady-state trajectories of the state-variables  $i$ ,  $i_g$  and  $v_c$  as well as the reference signals for the three pulse-width modulators. The calculation of these reference trajectories is discussed in the next section. One option is to calculate these trajectories off-line for a variety of different modulation indices and phase angles and to store the results in lookup tables. An alternative would be to calculate the reference trajectories on the fly by using modern high-performance microprocessors or FPGAs.

All small-signal quantities in Fig. 2 are indicated by  $\tilde{\cdot}$ . The aim of the LQR is to force the state variables of the physical system along the pre-calculated reference trajectories by making small adjustments to the duty cycles of the three pulse-width modulators. The LQR can thus be viewed as a small-signal controller. Under ideal conditions, all small-signal quantities are zero.

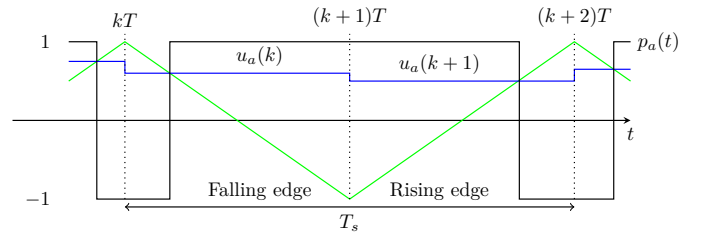


Fig. 3. PWM waveforms. Time instants  $kT$ ,  $(k+1)T$ ,  $(k+2)T$ , ... are the sampling points for all discrete-time signals.

### 2.3 Calculation of the steady-state reference trajectories

Asymmetrically-regularly sampled discrete-time control loops execute at twice the switching frequency  $f_s$  of the converter. The spectrum of pulse-width modulated signals consists of a fundamental component as well as sidebands of switching harmonics centred at integer multiples of the switching frequency (see Holmes and Lipo (2003)). As a result, the continuous-time state variables contain frequency components well above the Nyquist frequency of the loop. This results in a phenomenon referred to as ripple aliasing. Asymmetric-regular sampling overcomes this problem to a certain extent since, by sampling at the two peaks of the triangular carrier, inductor currents are usually sampled close to the centre of the current ripple. The sampled value of the particular current is thus a type of “running average” of the corresponding continuous-time current. However, it will later be shown that the same is not true for the capacitor voltages. Calculating the reference trajectories of the state-variables takes these high-frequency components into consideration and mitigates the effect of ripple aliasing.

In order to calculate the reference trajectories, it is assumed that the system of Fig. 1 is in the steady state and that the grid voltages are balanced with positive phase sequence. The first step is to determine the amplitude  $V_a$  and phase  $\phi_a$  of the fundamental component of the phase- $a$  converter output voltage  $v_{an}$ . Since the magnitude and phase of  $i_{ga}$  is specified by  $I_g^*$  and  $\phi_g^*$ , this can easily be accomplished by means of phasor analysis.

Recall that the amplitude of the triangular carrier is assumed to be 1. The phase- $a$  PWM reference waveform  $u_{ra}^*(kT)$  is thus given by  $u_{ra}^*(kT) = 2\frac{V_a}{V_d} \sin(\omega_g kT + \phi_a)$ , where  $\omega_g = 2\pi f_g$  is the angular frequency of the grid voltage.

One of the features of asymmetrically-regularly sampled PWM is the fact that the magnitude and phase of the fundamental component of the pulse-width-modulated waveform  $p_a(t)$  differ slightly from those of the reference waveform. A small correction to the amplitude of  $u_{ra}^*(kT)$  is made by solving for the fundamental component in Eq. (6.63) of Holmes and Lipo (2003), while the phase of  $u_{ra}^*(kT)$  is advanced by  $\frac{T}{2}$ . The phase- $b$  and phase- $c$  PWM references have the same amplitude as phase- $a$  but lag  $u_{ra}^*(kT)$  by  $\frac{2\pi}{3}$  rad and  $\frac{4\pi}{3}$  rad, respectively.

Space-vector centering is accomplished by applying a min-max argument (see Eq. (6.33) from Holmes and Lipo (2003)):

$$\begin{bmatrix} u_a^* \\ u_b^* \\ u_c^* \end{bmatrix} = \begin{bmatrix} u_{ra}^* \\ u_{rb}^* \\ u_{rc}^* \end{bmatrix} - \frac{\max(u_{ra}^*, u_{rb}^*, u_{rc}^*) + \min(u_{ra}^*, u_{rb}^*, u_{rc}^*)}{2} \begin{bmatrix} 1 \\ 1 \\ 1 \end{bmatrix}$$

This yields the steady-state PWM reference trajectories  $u_a^*(k)$ ,  $u_b^*(k)$  and  $u_c^*(k)$ .

The next step is to calculate the steady-state trajectory of the state vector  $\mathbf{x}(k) = [\mathbf{i}^T(k) \mathbf{i}_g^T(k) \mathbf{v}_c^T(k)]^T$ . Assume for the moment that all three grid voltages are zero.

The switching frequency  $f_s$  is chosen to be an integer multiple of 3 times the fundamental frequency  $f_g$  of the grid voltage. As a result of this choice, all the state variables are periodic in the steady-state with a fundamental frequency

of  $f_g$ . The steady-state trajectory of  $\mathbf{x}(k)$  is calculated by integrating Eq. (1) over one fundamental period and imposing this periodicity condition. Choose  $k = 1$  at the start of a fundamental cycle. The phase of the triangular carrier is chosen such that it coincides with the peak of the triangular carrier. Let  $\mathbf{x}(1)$  denote the state-vector at  $k = 1$ .

By integrating Eq. (1) over the first half of the switching period, during which the carrier is decreasing, it can be shown that

$$\mathbf{x}(k+1) = e^{TF} \mathbf{x}(k) + \mathbf{H}_f(u_a^*(k), u_b^*(k), u_c^*(k)), \quad (2)$$

where

$$\begin{aligned} \mathbf{H}_f(u_a^*(k), u_b^*(k), u_c^*(k)) &= 2\mathbf{F}^{-1} e^{\frac{T}{2}\mathbf{F}} \left\{ e^{\frac{T}{2}u_a^*(k)\mathbf{F}} \mathbf{G} \begin{bmatrix} 1 & 0 & 0 \end{bmatrix}^T \right. \\ &+ e^{\frac{T}{2}u_b^*(k)\mathbf{F}} \mathbf{G} \begin{bmatrix} 0 & 1 & 0 \end{bmatrix}^T + e^{\frac{T}{2}u_c^*(k)\mathbf{F}} \mathbf{G} \begin{bmatrix} 0 & 0 & 1 \end{bmatrix}^T \left. \right\} \\ &- \mathbf{F}^{-1} [e^{TF} + \mathbf{I}] \mathbf{G} \begin{bmatrix} 1 & 1 & 1 \end{bmatrix}^T. \end{aligned}$$

Integrating Eq. (1) over the second half (rising carrier) of the carrier yields

$$\mathbf{x}(k+1) = e^{TF} \mathbf{x}(k) + \mathbf{H}_r(u_a^*(k), u_b^*(k), u_c^*(k)), \quad (3)$$

where

$$\begin{aligned} \mathbf{H}_r(u_a^*(k), u_b^*(k), u_c^*(k)) &= -2\mathbf{F}^{-1} e^{\frac{T}{2}\mathbf{F}} \left\{ e^{-\frac{T}{2}u_a^*(k)\mathbf{F}} \mathbf{G} \begin{bmatrix} 1 & 0 & 0 \end{bmatrix}^T \right. \\ &+ e^{-\frac{T}{2}u_b^*(k)\mathbf{F}} \mathbf{G} \begin{bmatrix} 0 & 1 & 0 \end{bmatrix}^T + e^{-\frac{T}{2}u_c^*(k)\mathbf{F}} \mathbf{G} \begin{bmatrix} 0 & 0 & 1 \end{bmatrix}^T \left. \right\} \\ &+ \mathbf{F}^{-1} [e^{TF} + \mathbf{I}] \mathbf{G} \begin{bmatrix} 1 & 1 & 1 \end{bmatrix}^T. \end{aligned}$$

By consecutively applying these equations over one fundamental period, we obtain

$$\begin{aligned} \mathbf{x}(N) &= e^{NT\mathbf{F}} \mathbf{x}(1) + e^{(N-1)T\mathbf{F}} \mathbf{H}_f(u_a^*(1), u_b^*(1), u_c^*(1)) \\ &+ e^{(N-2)T\mathbf{F}} \mathbf{H}_r(u_a^*(2), u_b^*(2), u_c^*(2)) + \dots \\ &\dots + e^{T\mathbf{F}} \mathbf{H}_f(u_a^*(N-1), u_b^*(N-1), u_c^*(N-1)) \\ &+ \mathbf{H}_r(u_a^*(N), u_b^*(N), u_c^*(N)). \end{aligned}$$

By periodicity,  $\mathbf{x}(N) = \mathbf{x}(1)$ . Hence, solving for  $\mathbf{x}(1)$  yields

$$\begin{aligned} \mathbf{x}(1) &= [\mathbf{I} - e^{NT\mathbf{F}}]^{-1} \left\{ e^{(N-1)T\mathbf{F}} \mathbf{H}_f(u_a^*(1), u_b^*(1), u_c^*(1)) \right. \\ &+ e^{(N-2)T\mathbf{F}} \mathbf{H}_r(u_a^*(2), u_b^*(2), u_c^*(2)) + \dots \\ &\dots + e^{T\mathbf{F}} \mathbf{H}_f(u_a^*(N-1), u_b^*(N-1), u_c^*(N-1)) \\ &+ \left. \mathbf{H}_r(u_a^*(N), u_b^*(N), u_c^*(N)) \right\}. \end{aligned}$$

Once the value of  $\mathbf{x}(1)$  has been calculated, the steady-state trajectory of the state variables can be calculated over one fundamental cycle by consecutively applying Eqs. (3) and (2). These equations provide a solution of the complete non-linear system over one fundamental period, thereby taking the full non-linear behaviour of the pulse-width modulator into account.

The final step in the calculation is to use the principle of superposition to calculate the effect of the grid voltages on the steady-state trajectory of the state variables. To this end, assume that the three converter output voltages  $v_{an}$ ,  $v_{bn}$  and  $v_{cn}$  are zero. A simple phasor analysis can again be performed to calculate the steady-state trajectory of the state vector. By superposition, the resulting trajectory is superimposed on the trajectory  $\mathbf{x}(k)$ , calculated above, to obtain  $\mathbf{x}^*(k) = [\mathbf{i}^{*T}(k) \mathbf{i}_g^{*T}(k) \mathbf{v}_c^{*T}(k)]^T$ .

### 2.4 Small-signal model and discrete-time representation

A small-signal linearisation of the pulse-width modulated control loop is performed in this section. All small-signal quantities are indicated by  $\tilde{\cdot}$ .

### 3. CASE STUDY

Table 1. System parameters

Parameter	Symbol	Value
DC bus voltage	$V_d$	1 127 V
Filter inductance	$L$	30 $\mu\text{H}$
Filter capacitance	$C$	1.98 mF
Grid-side inductance	$L_g$	29.19 $\mu\text{H}$
Inductor ESR	$R$	54 m $\Omega$
Filter-capacitor ESR	$R_C$	0.667 m $\Omega$
Grid-side inductor ESR	$R_g$	1.1 m $\Omega$
Grid voltage (line-to-line)	$V_g$	690 V (RMS)
Grid frequency	$f_g$	50 Hz
Switching frequency	$f_s = \frac{1}{T_s}$	1 650 Hz
Nominal phase current	$I_{nom}$	4 132 A (RMS)

Fig. 4 shows the input signal  $u_a^*(k)$  to the pulse-width modulator of phase- $a$  as well as  $u_a^*(k)$  with a small-signal perturbation  $\tilde{u}_a(k)$  superimposed on it. The presence of this perturbation gives rise to small changes to the timing of the PWM pulse edges. The difference between the original PWM pulse train  $p_a^*(t)$  and the modified pulse train  $\tilde{p}_a(t)$  is a sequence of narrow rectangular pulses. These narrow rectangular pulses can be approximated by impulses as shown in the bottom graph of Fig. 4. The strength of each impulse is equal to the area of the narrow rectangle it represents, which is equal to the sampling period  $T$  multiplied by the value of the small-signal perturbation. This small-signal modelling approach was first published in Brown and Middlebrook (1981). Note that these impulses are not spaced equidistantly in time. In order to simplify the analysis, it is assumed that the impulses occur at the centre of each sampling period, i.e. at times  $(k + \frac{1}{2})T$ ,  $(k + \frac{3}{2})T$ , and so on. Most systems are insensitive to the exact placement of these impulses.

To obtain the model of the small-signal feedback loop, a few modifications to Fig. 2 are required: The reference trajectory generator is a feed-forward compensator, and all its output signals are set to zero in the small-signal circuit. The grid voltages are also set to zero. The pairs of pulse width modulators and switches in a phase leg of the converter are replaced by impulse generators, as described above. The aim of the LQR is then to regulate the small-signal state vector  $\tilde{\mathbf{x}}(k) = [\tilde{i}^T(k) \tilde{i}_g^T(k) \tilde{v}_c^T(k)]^T$  to zero.

The evolution of small-signal variables (at the sampling points) is described by the following discrete-time state-space representation:

$$\begin{aligned} \tilde{\mathbf{x}}(k+1) &= e^{TF} \tilde{\mathbf{x}}(k) + T \int_0^T e^{(T-\tau)F} \delta\left(\tau - \frac{T}{2}\right) \mathbf{G} \tilde{\mathbf{u}}(k) d\tau \\ &= e^{TF} \tilde{\mathbf{x}}(k) + T e^{\frac{T}{2}F} \mathbf{G} \tilde{\mathbf{u}}(k), \end{aligned}$$

where  $\tilde{\mathbf{u}}(k) = [\tilde{u}_\alpha(k) \tilde{u}_\beta(k)]^T$ , and  $\delta(t - t_0)$  represents an impulse of strength 1 at time  $t_0$ . This is the familiar impulse invariance continuous-to-discrete time transformation of the multiple-input multiple-output plant with an additional half-sample delay. The discrete-time small-signal model can now be written in the form:

$$\tilde{\mathbf{x}}(k+1) = \mathbf{A} \tilde{\mathbf{x}}(k) + \mathbf{B} \tilde{\mathbf{u}}(k),$$

where

$$\mathbf{A} = e^{TF} \quad \text{and} \quad \mathbf{B} = T e^{\frac{T}{2}F} \mathbf{G}. \quad (4)$$

This linear discrete-time model will be used in the design of the LQR, which is the subject of the next section.

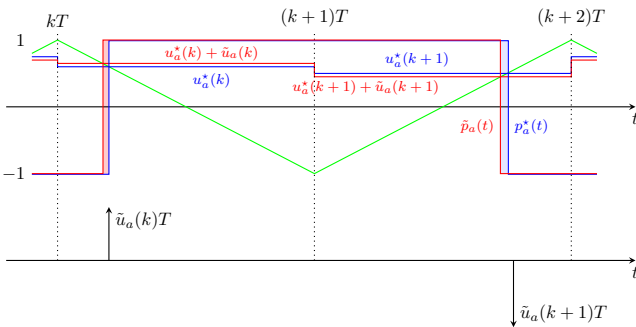


Fig. 4. Derivation of the small-signal model. The narrow rectangular pulses are modelled by impulses.

Table 1 lists the system parameters of the high-power grid-connected converter that will be used as a case study.

#### 3.1 Controller design

The LQR cost function is defined as

$$J = \sum_{k=1}^{\infty} (\tilde{\mathbf{x}}^T(k) \mathbf{Q} \tilde{\mathbf{x}}(k) + \tilde{\mathbf{u}}^T(k) \mathbf{R} \tilde{\mathbf{u}}(k) + 2\tilde{\mathbf{x}}^T(k) \mathbf{N} \tilde{\mathbf{u}}(k)),$$

where  $\tilde{\mathbf{x}}(k)$  is the small-signal state vector.

Matrix  $\mathbf{Q}$ , which determines the penalty on the small-signal state variables, was chosen as

$$\mathbf{Q} = \text{diag}(0.2, 0.2, 1, 1, 0.1, 0.1).$$

Since the primary objective is to track the grid current references, the relatively large weight of 1 was placed on the grid currents, and smaller weights of 0.2 and 0.1 were used for the inductor currents and capacitor voltages, respectively. Matrix  $\mathbf{R}$  penalizes the control effort and was chosen as  $1000 \mathbf{I}_2$ , where  $\mathbf{I}_2$  is the  $2 \times 2$  identity matrix. Matrix  $\mathbf{N}$  was chosen as zero.

#### 3.2 Simulation results

In this section, we provide simulation results to verify the performance of the proposed control scheme. The resonance frequency (of the transfer function from the converter's output voltage to the grid current) is at  $f_1 = 930$  Hz. This is more than half the switching frequency  $f_s$  of 1 650 Hz. The grid current leads the grid voltage by  $30^\circ$ , i.e.  $\phi_g^* = 30^\circ$  in Fig. 2.

Fig. 5 shows the response of the loop to a step in the amplitude of the reference current. The amplitude of the reference current  $I_g^*$  is stepped from 2.8284 kA to its nominal value of 5.8435 kA at  $t = 25$  ms. The top graph of Fig. 5 shows the simulated grid currents as well as the sinusoidal reference currents. It can be seen that the grid currents respond quickly and without significant overshoot to the reference step. Fig. 5 also shows the small-signal corrections made by the LQR. Only very small corrections are made during steady-state operation. Larger corrections are made during the startup transient and the reference step, when the regulator forces the state variables to track the steady-state reference trajectories. In both cases, a settling time of approximately 3 ms is observed.

Fig. 5 also shows the inductor currents and capacitor voltages along with their respective reference trajectories.

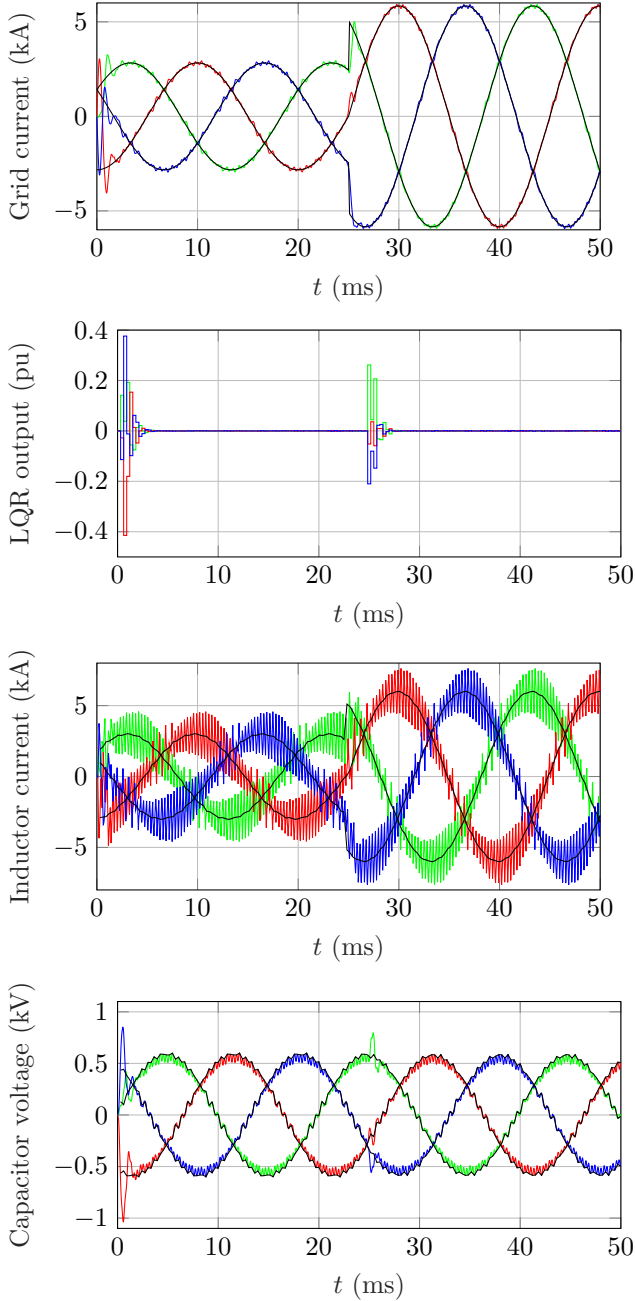


Fig. 5. Simulated results with a reference step at 25 ms. Reference trajectories are shown in black.

Closer investigation reveals that the continuous-time inductor currents intersect the reference trajectories at the sampling points (upper and lower peaks of the PWM carrier) during steady-state operation. The capacitor voltages also intersect their reference trajectories at the sampling points. It is interesting to note that, unlike the inductor currents, these sampling points are not in the centre of the capacitor voltage ripple. Instead, the reference trajectories correspond to the outer envelopes of the capacitor voltage.

One of the disadvantages of conventional linear controllers that contain integrators is the phenomenon of integrator wind-up during transients, when the pulse-width modulators may be driven into over-modulation. Special anti wind-up techniques (see for instance Kothare et al. (1994) and Goodwin et al. (2001)) have been developed to mit-

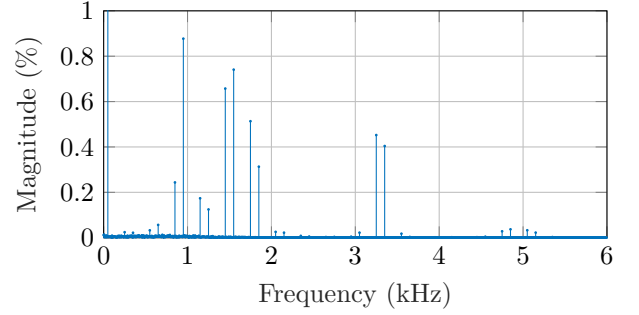


Fig. 6. Grid current spectrum with  $I_g^*$  set to its nominal value. The harmonic magnitudes are shown as a percentage of the fundamental.

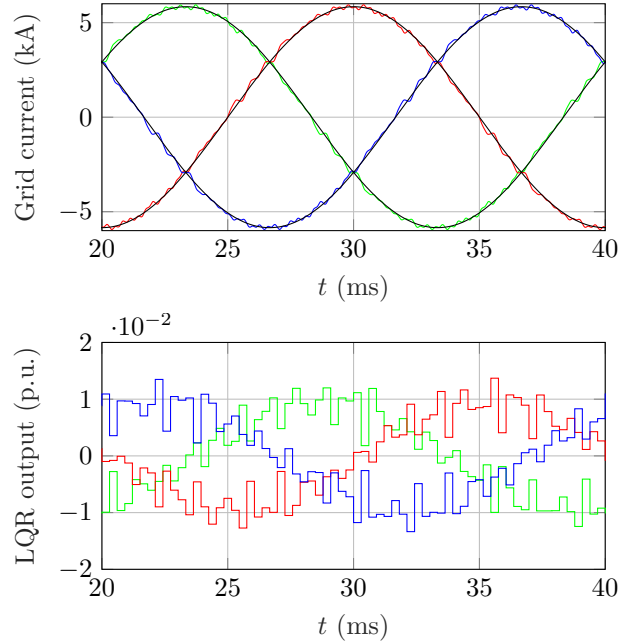


Fig. 7. Operation with non-ideal system parameters.

igate the effects of integrator wind-up. Since the control law applied by the LQR is just a linear combination of state variables, it doesn't suffer from this problem.

Fig. 6 shows the spectrum of the grid current with  $I_g^*$  set to its nominal value. The fundamental component of the grid current has an amplitude of 5.8450 kA and a phase of  $30.0013^\circ$ , which compares very well with the reference values of 5.8435 kA and  $30^\circ$ . The amplitudes of the harmonics in Fig. 6 are indicated as a percentage of the fundamental component's amplitude. The total harmonic distortion of the grid current is 1.8636%. The largest harmonic of the grid current occurs at a frequency of 950 Hz, which is very close to the resonant peak of the *LCL* filter's transfer function from converter output voltage to grid current which is located at 930 Hz, as mentioned earlier.

In order to evaluate the robustness of the controller with respect to parameter variations, the grid inductance  $L_g$  of the physical system was reduced by 20% from its nominal value of  $29.19 \mu\text{H}$  to  $23.352 \mu\text{H}$  without changing the control model. Fig. 7 shows the grid current with  $I_g^*$  set to its nominal value. Fig. 7 also shows the output signal of

the LQR. The fundamental component of the grid current has an amplitude of 5.8455 kA and a phase of  $30.8001^\circ$ , which still compare very well with their reference values. Fig. 8 shows the grid current spectrum. A comparison with Fig. 6 shows a noticeable increase in the magnitude of the harmonics. The total harmonic distortion of the grid current increased from 1.8636% to 2.4765%. This increase is partly due to the fact that the smaller grid-side inductor provides less attenuation of the switching harmonics. Another simulation was performed where the model of the system was updated with the correct value of  $L_g = 23.352 \mu\text{H}$ . In this case the THD of the grid current was 2.172%.

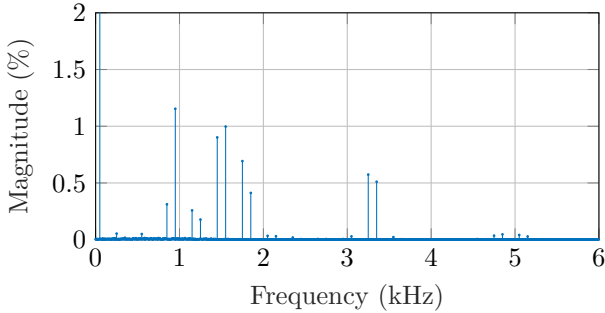


Fig. 8. Grid current spectrum with non-ideal system parameters. The harmonic magnitudes are shown as a percentage of the fundamental.

#### 4. CONCLUSIONS

This paper presented a trajectory-based controller for a grid-connected converter with an *LCL* filter. The simulation results showed that the controller exhibits very good performance during both steady-state and transient conditions.

The main advantage of this controller is that it can operate at switching frequencies below twice the resonance frequency of the filter. For classic PI-based controller designs with an additional control loop that provides active damping of the filter resonance, it is widely accepted that the switching frequency must be at least three times the resonance frequency. Lower switching frequencies reduce the switching losses of the converter and thus increase the efficiency. Alternatively, when operating the converter system at the typically used switching frequency, the LQR allows one to increase the resonance frequency, thus reducing the filter components. This increases the power density, reduces the weight and lowers the price of the converter system. Other advantages include the simplicity of designing the LQR as well as the fact that the proposed approach does not require an anti wind-up scheme.

Future research will focus on including both state and actuator constraints and reformulating the problem as a constrained quadratic optimisation problem. Unlike the approach presented in Mariethoz and Morari (2009), where the non-linear behaviour of the pulse-width modulator was modelled by means of a piecewise affine system, the proposed approach will result in a constrained linear system which can be controlled by solving a quadratic programme.

#### REFERENCES

- Brown, A.R. and Middlebrook, R. (1981). Sampled-data modeling of switching regulators. In *Power Electronics Specialists Conference, 1981 IEEE*, 349–369.
- Dahono, P.A. (2002). A control method to damp oscillation in the input LC filter. In *2002 IEEE 33rd Annual IEEE Power Electronics Specialists Conference. Proceedings (Cat. No.02CH37289)*, volume 4, 1630–1635.
- Dannehl, J., Fuchs, F.W., Hansen, S., and Thogersen, P.B. (2010). Investigation of active damping approaches for PI-based current control of grid-connected pulse width modulation converters with LCL filters. *IEEE Transactions on Industry Applications*, 46(4), 1509–1517.
- Goodwin, G., Graebe, S., and Salgado, M. (2001). *Control system design*. Prentice Hall.
- Holmes, D. and Lipo, T. (2003). *Pulse Width Modulation for Power Converters (Principles and Practice)*. IEEE Press Series on Power Engineering.
- Kothare, M.V., Campo, P.J., Morari, M., and Nett, C.N. (1994). A unified framework for the study of anti-windup designs. *Automatica*, 30(12), 1869–1883.
- Liserre, M., Dell’Aquila, A., and Blaabjerg, F. (2004). Genetic algorithm-based design of the active damping for an LCL-filter three-phase active rectifier. *IEEE Transactions on Power Electronics*, 19(1), 76–86.
- Loh, P.C. and Holmes, D.G. (2005). Analysis of multi-loop control strategies for LC/CL/LCL-filtered voltage-source and current-source inverters. *IEEE Transactions on Industry Applications*, 41(2), 644–654.
- Mariethoz, S. and Morari, M. (2009). Explicit model-predictive control of a PWM inverter with an LCL filter. *IEEE Transactions on Industrial Electronics*, 56(2), 389–399. doi:10.1109/TIE.2008.2008793.
- Nieuwstadt, M.J.V. and Murray, R.M. (1997). Real-time trajectory generation for differentially flat systems. *International Journal of Robust and Nonlinear Control*, 8(11), 995–1020.
- Parker, S.G., McGrath, B.P., and Holmes, D.G. (2014). Regions of active damping control for LCL filters. *IEEE Transactions on Industry Applications*, 50(1), 424–432.

#### Appendix A. STATE-SPACE MATRICES

$$\mathbf{F} = \begin{bmatrix} -\frac{RC+R}{L} & 0 & \frac{RC}{L} & 0 & -\frac{1}{L} & 0 \\ 0 & -\frac{RC+R}{L} & 0 & \frac{RC}{L} & 0 & -\frac{1}{L} \\ \frac{RC}{L_g} & 0 & -\frac{RC+R_g}{L_g} & 0 & \frac{1}{L_g} & 0 \\ 0 & \frac{RC}{L_g} & 0 & -\frac{RC+R_g}{L_g} & 0 & \frac{1}{L_g} \\ \frac{1}{C} & 0 & -\frac{1}{C} & 0 & 0 & 0 \\ 0 & \frac{1}{C} & 0 & -\frac{1}{C} & 0 & 0 \end{bmatrix}$$

$$\mathbf{G} = \begin{bmatrix} \frac{V_d}{2L} & 0 \\ 0 & \frac{V_d}{2L} \\ 0 & 0 \\ 0 & 0 \\ 0 & 0 \end{bmatrix} \quad \mathbf{H} = \begin{bmatrix} 0 & 0 \\ 0 & 0 \\ -\frac{1}{L_g} & 0 \\ 0 & -\frac{1}{L_g} \\ 0 & 0 \\ 0 & 0 \end{bmatrix}$$